Nicolás Herrera-Sandoval
Daniel Molinero-Hernández
Sergio Galván-González ✉
Cristóbal Camacho-Arriaga
Carlos Rubio-Maya
Jesús Pacheco-Ibarra

https://doi.org/10.21278/TOF.493053723
ISSN 1333-1124
eISSN 1849-1391

NUMERICAL SHAPE OPTIMISATION OF AN ISOLATED HYDRAULIC DIFFUSER

Summary

In the draft tube of hydraulic turbines, the remaining kinetic energy of the runner is transformed into pressure mainly due to its diffuser geometry. Recognizing that the divergence section reduces flow velocity and the straight duct promotes flow uniformity, determining the exact relation between these sections for a fixed space in a diffuser is crucial to improving the overall performance of the diffuser. To find this relation, we designed an automatic optimisation process by coupling computational fluid dynamics (CFD) software to a distributed genetic algorithm that manipulated a single diffuser parameter to minimise its energy losses. By using this method, the best geometries were determined by employing a low-fidelity CFD model, but the fluid flow analysis was done on a high-fidelity one. The results show that the precise relation between the divergence and the duct for a defined inlet velocity profile in a diffuser can minimise the energy losses, recovering up to 90% of the mean static pressure.

Key words: *diffuser; CFD, draft tube; numerical optimisation; genetic algorithm*

1. Introduction

To gain efficiency in the draft tube of a hydraulic turbine, the remaining kinetic energy that enters the tube needs to be converted into pressure. This conversion occurs mainly at the inlet of the draft tube, i.e. at the conical part called the diffuser [1-3]. In the last century, some direct experimental approaches to evaluate the performance of this device demonstrated that its pressure recovery is highly dependent on the conditions of the inlet flow and its design parameters as diffuser angle, area ratio (AR), length ratio (LR), wall shape and cross section [4-6]. More specifically, it is established in [7] that through these design parameters a higher performance might be obtained, either by increasing the amount of diffusion, decreasing any non-uniformity in the inlet velocity profile, or making the diffusion more efficient, thus reducing overall losses across the diffuser.

Since researchers achieved only minor progress with direct experimentation, they had to consider numerical tools such as CFD to interpret and understand the flow behaviour generated by the modification of the diffuser design parameters [8-12].

The systematic manipulation of these design parameters required the implementation of numerical algorithms [13-14], which, when coupled with CFD software, created an optimisation based on the CFD method [15]. This approach was applied in basic research to isolated diffusers to enhance their performance. The divergent angle and the wall shape were used by [16-19] as design variables for a duct-divergence-duct diffuser configuration. It was also applied to improve the performance of diffusers functioning directly as draft tubes, such as the redesign of the T99 diffuser cross section for two distinct operational conditions [20-21] or the use of various angles for three specific diffuser shapes: straight, trumpet, and bell [22-23], and the reconstruction of the wall shape of the divergent part of a divergent-duct diffuser using diverse approaches [24]. However, these studies only used the pressure recovery factor to gain performance and ignored the diffusive or dissipative impact on the diffuser performance.

For a draft tube redesign where the AR is a design variable, it is demonstrated that the diffusion effect is mainly responsible for the increase in pressure recovery, regardless of the dissipative rise [25]. However, in most reaction turbine installations, the coupling between the runner and the elbow part of the draft tube is fixed. These geometrical restrictions limit the diffusion effects on the inlet flow provided by the runner. Therefore, the only way to improve the diffuser performance is by making the diffusion more efficient by reducing the flow energy losses along it.

Therefore, this paper aims to minimise only the dissipative part of the pressure recovery instead of using the whole parameter set as the objective function, as has usually been done. The modification of the flow dissipation could be made not only by modifying the position of the angle in a divergence-duct configuration but also by modifying the entry pipe length, even in a better way than only a divergence. Besides, the divergent wall may vary in size and shape, from a straight line to several different types of curves, looking to increase the swirling intensity, and making the boundary layer more capable of radial momentum transfer.

Thus, to determine the configuration and wall shape that the diffuser requires to minimise the flow dissipation and maximise the flow diffusion, an automatic optimisation process was designed, coupling software from different disciplines. Additionally, the best determined geometries were analysed to understand why each component of the pressure recovery equation, dissipation, and diffusion was affected, and how the engineering quantities that govern the diffuser performance along it were modified.

According to the numerical results obtained by this study, we infer that the re-design of a diffuser as the link between the runner exit and the elbow of the draft tube could correct the evolution of swirling flows created by a runner in different operational points of the turbine. This flow correction could avoid a sudden and unexpected drop in discharge efficiency or even improve it.

2. Method

A shell script executed the search for the optimal shape of the diffuser by coupling codes of different disciplines, Fig. 1. An optimisation algorithm controls the automatic process [26].

The process begins with a proposal of a new design variable value. This value is then used to generate a coordinate file [27] containing information about the diffuser wall shape and LR. Subsequently, the coordinate file is used to create the domain mesh [28], followed by a CFD analysis [29]. The numerical results are then evaluated to assess the performance of the studied geometry [27]. This information is then fed back to the optimisation algorithm. The overall process iterates until it reaches the pre-determined number of cycles specified during the optimisation algorithm setup. This section details the elements and conditions defined for each step of the optimisation process.

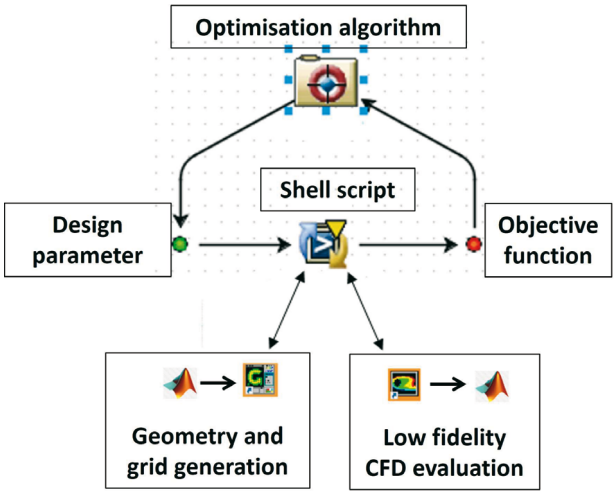

Fig. 1 Optimisation process guided by the shell program

2.1 Diffuser geometries

Fig. 2 presents two configurations considered to create the diffuser geometry: the divergence section followed by a parallel pipe (div-duc) and a straight section followed by a divergence part (duc-div). In the meridional half-plane, five fixed points, *a*, *b*, *d* and *e*, and *c*, outlined the geometry of the diffuser. Since the A_{in}/A_{out}=4 and L/D=5.3 are geometrical parameters of the original diffuser, point $c(y, z_i)$ turned out to be the design variable with only one degree of freedom along the *z*-axis. This action should create an axisymmetric surface with different div-duc or duc-div relations through l/L. Revolving this surface around the *z*-axis created the computational domain.

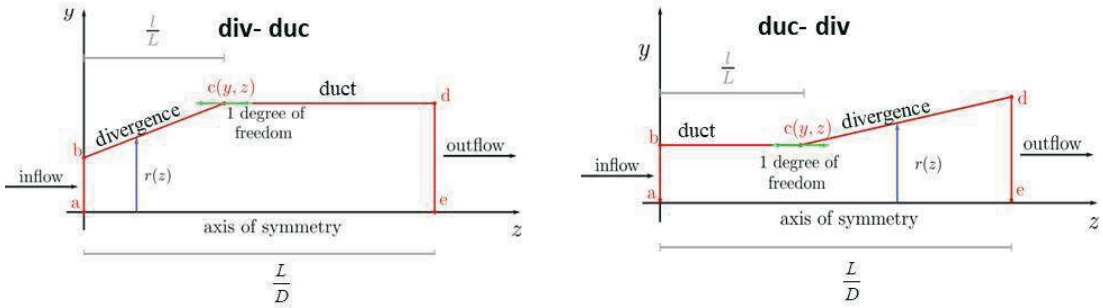

Fig. 2 Geometric configurations of the diffuser

2.2 Wall-shape divergence

The diffuser divergence was shaped along the radius based on the theory of the bell mouth draft tube [30]. Its performance depends on the profile of its cross sections, which should provoke a more uniform flow distribution. Eq. (1) defines the axial velocity in the diffuser, provided that it is the potential flow of an ideal fluid.

$$Va = \frac{\mathrm{d}z}{\mathrm{d}t} = \frac{\mathrm{d}Q}{2\pi r \mathrm{d}r} = \frac{1}{r^2} K \tag{1}$$

Additionally, different wall shape divergences are obtained by assuming various values for the radial component of the velocity $Vr=\mathrm{d}r/\mathrm{d}t$.

For example, when $Vr=rC$, Prasil's hyperbola (PH), where:

$$r = \sqrt{\frac{z_1 - C_2}{C_1}} \tag{2}$$

When $Vr=C$, the constant expansion hyperbola (EH), where:

$$r = \frac{C_1}{z - C_2} \tag{3}$$

When $Vr=C/r$, the logarithmic hyperbola (LH), where:

$$r = 10^{\frac{z-C_2}{C_1}}, \tag{4}$$

and when $Vr=C/r^2$, the straight line (SL), where:

$$r = \frac{z - C_2}{C_1} \tag{5}$$

The coordinate z modifies the divergent wall shape through the radius from $r(0)$ to $r(c)$ in the div-duc configuration, Fig. 2 (left), and from $r(c)$ to $r(L)$ in the duc-div configuration, Fig. 2 (right). C_1 and C_2 are constants obtained when the initial conditions are set up for $r(z)$. Only one design variable or control point, c_i, was constrained along the z-coordinate to establish the length of the curve that defined the wall shape.

2.3 Low-fidelity CFD model

Since the time of a complete optimisation process depends on the duration of each single CFD evaluation, the model complexity must be speed up as much as possible. A grid convergence study developed by [31] on the Turbine 99 draft tube demonstrated that a low-fidelity CFD model can reduce this complexity. This model is at the lowest limit of the asymptotic range but maintains the same constant near-wall grid points as the finest mesh.

In a previous study, a low-fidelity CFD model for such an optimisation process, as defined by [25], was found to be operating at the lowest limit of the asymptotic range using Richarson's extrapolation as in [32]. It consists of 47,124 elements with a grid error of 9.05%, but what is interesting is that it uses the same standard logarithmic rough wall function at the walls $y^+= 67.4416$ as the finest grid, making it a unique and efficient tool for our purposes.

The commercial finite volume-based software Fluent [29] defined the numerical setup of the model. Also, the diffuser model contains the same boundary conditions that were established in [25] and [33]: at the inlet section, a radial distribution of each velocity component, i.e. axial (V_a), radial (V_r), and tangential (V_t), through a free vortex approach, and at the outlet section, instead of a fixed constant pressure.

Thus, this reliable 3D CFD diffuser model, previously verified in a grid convergence study, was used to execute the low-fidelity simulations as a strategy to reduce the total computational time of the optimisation process.

2.4 Single objective-function

Eq. (6) defines diffuser performance as a mathematical model composed of two terms: flux diffusion and energy dissipation [7]. If the diffuser performance is to be improved through the pressure recovery coefficient, it would be convenient to study both sides of the equation separately, the flow uniformity and the total pressure losses.

$$Cp_{sh} = \alpha_{in}\left[1 - \frac{\frac{\alpha_{out}}{\alpha_{in}}}{AR^2}\right] \tag{6}$$

where *sh* determines the equation defined by [7], the first term defines the diffusion, and it is a result of the inlet and exit axial velocity profiles shapes α_{out} and α_{in} given by Eq. (7).

$$\alpha = \frac{1}{AV^3}\int_A v_a^3 \mathrm{d}A \tag{7}$$

The second term, ζ, defined by Eq. (8), represents the losses occurring within the diffuser due to the viscous effects as the flow travels downstream the diffuser.

$$\varsigma = \frac{\frac{1}{A_{in}}\int_{in} P_t \mathrm{d}A - \frac{1}{A_{out}}\int_{out} P_t \mathrm{d}A}{\frac{1}{2}\rho\left(\frac{Q}{A_{in}}\right)^2} \tag{8}$$

where P_t is the total pressure, and A_{in} and A_{out} are the areas at the inlet and outlet, respectively. The total pressure is given by $P_t = P + 0.5(u^2 + v^2 + w^2)$, with u, v and w as the Cartesian components of the velocity and P as the static pressure.

Since this analysis aims to understand the effect of the optimised diffuser shapes on diffusion and dissipation while the flow passes along it, the global quantities will be weighted by the area at several diffuser cross sections.

In this practical situation, we consider the diffuser separated from the draft tube as an isolated device, and its dimensions (AR and LR) fixed. Also, since the inlet velocity profile is pre-established, the only way to improve the diffuser performance through Eq. (6) remains in the viscous effects employing ζ as a single-value objective function, which is very sensitive to dynamic pressure variations provoked by the radial distribution of the velocity components along the diffuser [34]. This selection should greatly diminish the code running times, shortening, in turn, the overall optimisation process.

2.5 Set up of the numerical algorithm

From the advanced version of the traditional genetic algorithm (TGA) described and used by [35-36], [26] presents a multi-island genetic algorithm (MIGA), which incorporates parallel islands with sub-populations to diversify the search for an optimum.

We established ten islands in the MIGA with two designs for the div-duct process and four for the duct-div process. Thus, each generation was composed of a population of twenty and forty designs for each process. The usual genetic operations (selection, reproduction, and mutation) were performed separately on each island for twenty-five and fifteen generations, Table 1.

Table 1 Main parameters of the MIGA

Parameters	div-duc	duc-div
Number of islands	10	10
Size of sub-populations	2	4
Number of generations	25	15
Evaluations	500	600

A further operation called migration transferred some individuals from one island to another at specific intervals of generations to increase the geometric diversity of the diffuser. Thus, to complete each optimisation process, the CFD software must execute five hundred and six hundred evaluations.

2.6 Simultaneous CFD evaluations

If a machine had executed each optimisation process serially, the computational time required would have been enormous. Thus, the MIGA had to be implemented in a local network to distribute each CFD evaluation to a corresponding node to achieve their parallelism. In this

network, the controller node permitted access to ten calculating nodes with eight central processing unit (CPU) cores, 4.0 GHz, and 16 GB of RAM. Thus, by simultaneously evaluating ten CFD models, the distributed cluster significantly reduced the computational time of the optimisation process.

3. Optimisation results

The optimisation process minimised the objective function for each diffuser configuration, div-duc and duc-div, and each wall shape (SL, LH, EH, and PH). Fig. 3 shows the runs where l/L represents the position of point $c(y, z_i)$ according to Fig. 2. This point determines the length of the divergence or the duct. The schematic representation of each complete optimisation process illustrates how the robust algorithm reached a practical solution without having a local minimum for each optimisation process.

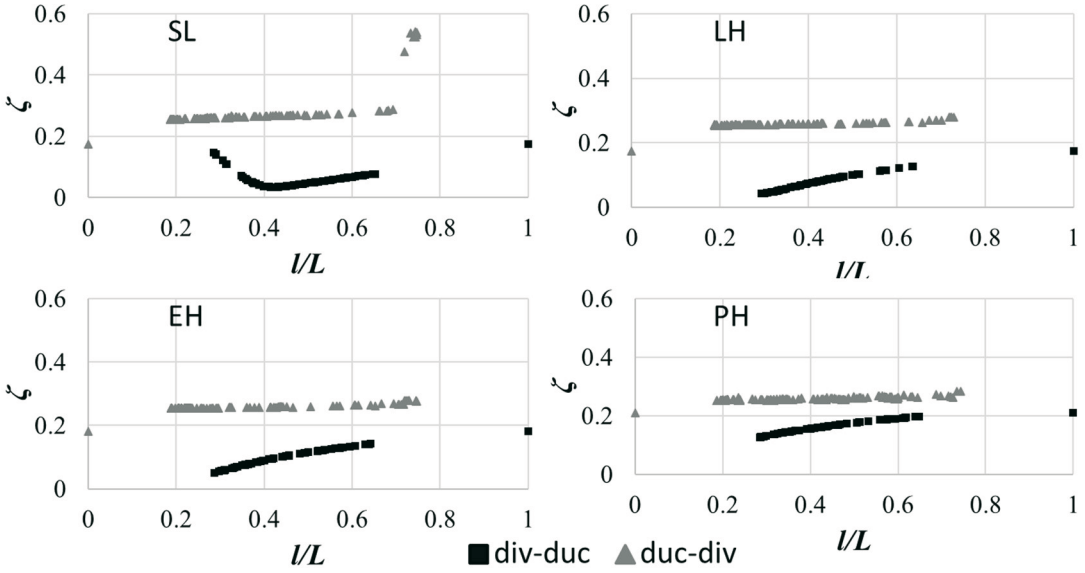

Fig. 3 Optimisation process of the diffuser for each geometry and wall-shape

The runs using the div-duc configuration allowed reducing the energy losses for the four types of wall shapes. The SL wall shape reached its minimum value when l/L=0.42. On the other hand, for the duc-div wall shapes, the runs could not minimize the objective function in the research space. The complete divergence of the diffuser was reached for the duc-div configuration when l/L=0 and for the div-duc configuration when l/L=1.

The plots of the entire processes test whether the divergence at the diffuser inlet needs a precise length when the SL wall shape is used to reach minimal energy loss. Similar ascending-descending behaviour for the SL divergence is reported by [20] concerning the diffuser angle. Thus, this result confirms that depending on the inlet flow conditions, an exact diffuser angle should exist to minimise the energy loss [37].

3.1 Optimised geometries

Fig. 4 presents the diffuser geometries that reached the lowest values of the objective function during the corresponding optimisation process.

With the divergence placed at the inlet of the diffuser, the SL wall shape required almost one-half of the diffuser length to minimise the energy losses with an exact angle of 12.51°. Instead, l/L is almost constant using any wall shape. When placing the duct at the inlet of the diffuser, l/L preserved virtually the same value despite the wall shape used in the divergent part.

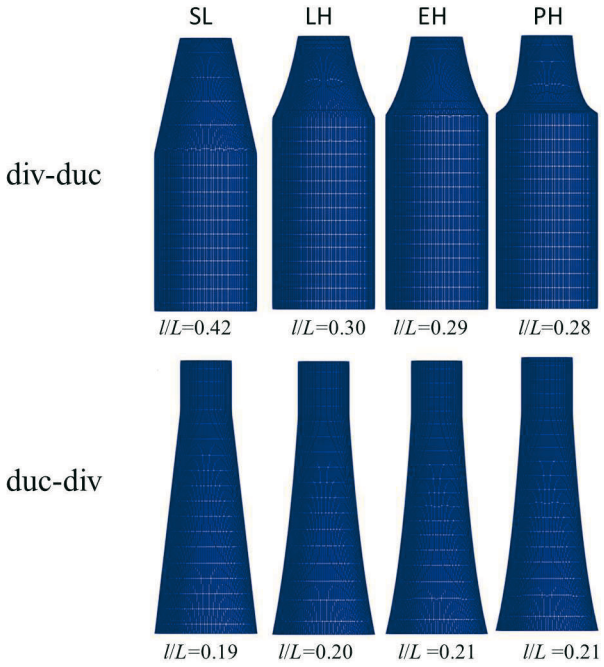

Fig. 4 Best diffuser geometries obtained by the optimisation process

4. Performance evaluation of the best diffuser geometry

The post-processing of the numerical flow field of each model allowed us to determine the proportion of diffusion, dissipation, and uniformity of the flow generated by the diffuser designs and how these flow characteristics influenced the diffuser performance. Fig. 5 presents all these results.

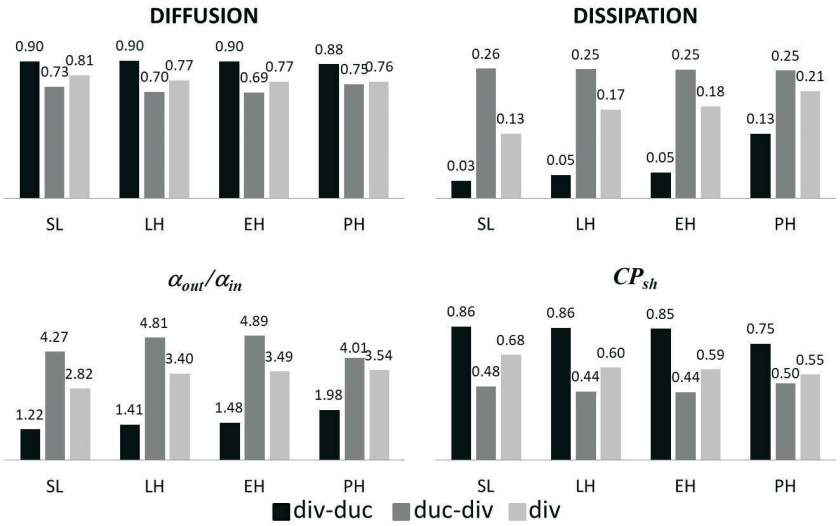

Fig. 5 Diffuser performance using Eq. (6)

The left side of Eq. (6) gives the amount of diffusion generated by the selected diffuser. The duc-div configuration permitted the highest diffusion. The duct placed at the inlet of the diffuser, i. e. the duc-div configuration, needs high curved walls to increase the fluid diffusion, i.e. PH. With only the divergence, the diffuser fluid dissipation was better than with the duc-div configuration but lower than the one with the div-duct configuration. α_{out}/α_{in} represents the distortion reached by the inlet velocity profile along the diffuser, Eq. (7).

The evaluation of Eq. (8) shows that the div-duc configuration always generates the lowest flow distortion. Besides, the divergent part placed at the inlet of the diffuser always

provokes the lowest dissipation. Further, the diffuser presents higher losses if it has the duct at the beginning or it only has the divergence.

Equation (6) permitted the evaluation of the diffuser performance (Cp_{sh}) reached by the different configurations and wall shapes. Despite the efficient diffusion expressed by the curved walls in the duc-div and div configurations, these diffuser shapes significantly affected the diffuser's overall performance. Thus, the SL wall shape achieved the best performance by minimizing the flow dissipation.

The results presented in this section confirm that the overall performance of the diffuser is increased by reducing the fluid dissipation instead of increasing the flow diffusion [7]. Also, this condition can be reached by an exact relation between the divergence and the duct of the diffuser.

5. Flow analysis along the optimised diffusers

Due to the coarse discretisation grid, premature interruption of the iterative solution, or computer round-off errors of the CFD model used during the optimisation process, the optimised geometries could be prone to a certain amount of numerical inaccuracy. Thus, the diffuser's CFD model was improved not only to correct all these inconveniences but also to achieve a higher resolution of the flow field created by the optimised geometries.

5.1 High-fidelity CFD model

While a low-fidelity CFD analysis was executed during the design iterations, a high-fidelity CFD analysis should evaluate the best designs, mainly to determine how the geometric characteristics impacted the fluid flow along the diffuser, validating its final design. However, solving the turbomachinery CFD problems with high-fidelity resolution requires computational power and memory bandwidth, which exceeds the features of the fastest multi-core CPUs.

As a massively parallel "co-processor" of the CPU, [38] adapted a general purpose graphics processor unit (GPGPU) to obtain a significant speedup simulation on the T99 draft tube, a 3D turbo-machinery well-known benchmark, which is a challenge for industrial CFD applications. However, to take advantage of its tremendous computing power, this hardware requires an open and parallelizable CFD software and an intermediate low-level interface able to transfer data between the CPU and GPGPU. The open field operation and manipulation (OpenFOAM) code gives us this opportunity as it provides a flexible simulation platform by mimicking the form of partial differential equations, and it runs in parallel using automatic/manual domain decomposition according to the solver activated [39]. The RapidCFD library is the interface used to couple the (OpenFOAM) CFD software, installed on the CPU, with the GPGPUs and to execute the entire simulation in parallel.

Thus, in spite of the high rotational, fluctuating, and non-uniform flow solved in the T99 draft tube CFD model, this approach proved its speed and reliability in the calculations. Due to the flow similarities with the diffuser, the same CFD characteristics were used to create a high-fidelity CFD model to execute simulations on the optimised diffuser geometries. The solver application simpleFoam solved an average grid size of 1.4 million cells for all cases in the steady state with double floating precision. The order of discretisation for gradient terms, convective terms, Laplacian terms, point-to-point interpolations, and gradient normal to cell faces was second order.

The linear solver for the pressure P discretized equation was preconditioned conjugate gradient (PCG) and preconditioned biconjugate gradient (PBiCG) for velocity V. Also, the PBiCG linear solver solved the κ and ε standard turbulence model. The approximate inverse (AINV) preconditioner solved the preconditioning of matrices for all quantities (P, V, κ, and ε). The semi-implicit method for pressure-linked equations (SIMPLE) algorithm solved the p-V equations system. The residual target was 1×10^{-03}.

Thus, the major benefit of using this open-source CFD software instead of a commercial one to solve this high-fidelity CFD model was that it permits the addition of new libraries, such as

RapidCFD, to activate additional hardware. Also, the computational power and memory bandwidth of the GPUs exceed the features of the fastest multi-core CPUs and can be considered equivalent to a small HPC cluster.

5.2 Analysis of the flow field

The flow behaviour along the diffuser was evaluated through five quantities using its corresponding optimised high-fidelity CFD model.

5.2.1 Energy loss coefficient

Fig. 6 shows the evolution of the energy loss coefficient along the diffuser given by Eq. (8). To visualize the variation of this quantity along the diffuser concerning the inlet section, the subindex out represents the evaluation of the performance quantity in the actual cross section.

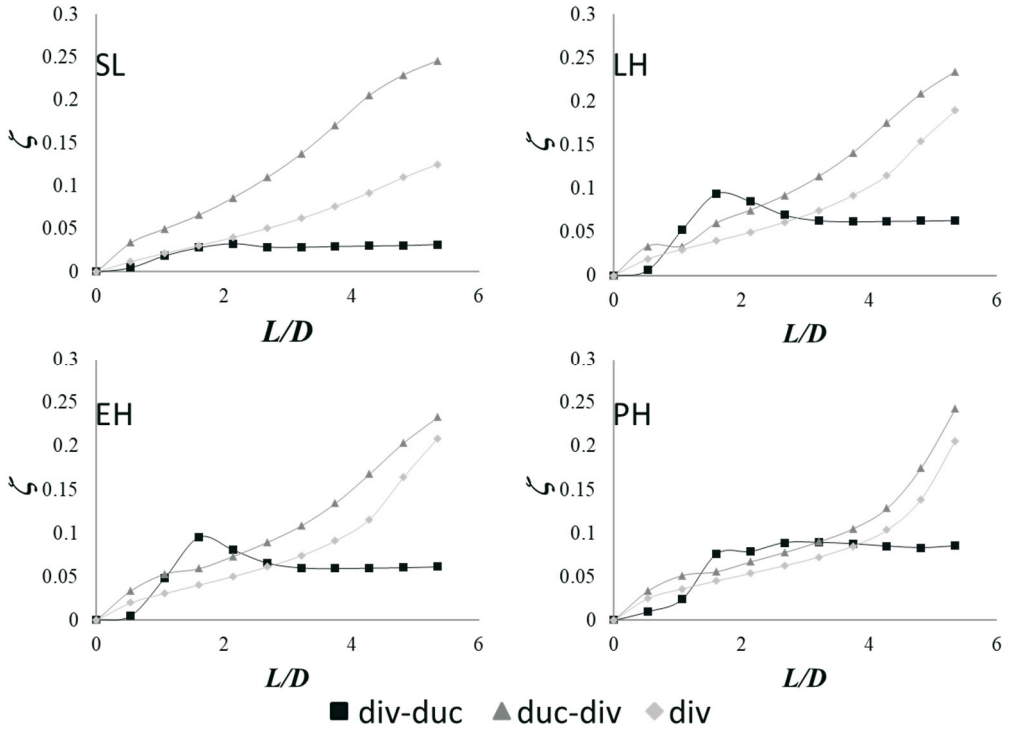

Fig. 6 Energy losses along the diffuser

In the div-duc configuration, the divergent part of the diffuser increases the energy loss. However, the duct held or decreased this value until its exit. A straight wall generated a lower loss coefficient than the curved walls. Using only divergent diffusers (div) or with a parallel pipe followed by the divergence (duc-div), the energy losses increased almost proportionally despite the diffuser wall shape.

5.2.2 Mean pressure recovery factor

Equation 9 calculates the mean-pressure-recovery coefficient changes in relation to the inlet cross section along the diffuser when it uses different divergent wall shapes.

$$Cp_m = \frac{\frac{1}{A_{out}}\int_{out} P\mathrm{d}A - \frac{1}{A_{in}}\int_{in} P\mathrm{d}A}{\frac{1}{2}\rho\left(\frac{Q}{A_{in}}\right)^2} \tag{9}$$

Fig. 7 shows that the Cp_m, which indicates the degree of conversion of kinetic energy into static pressure, reached its highest values using the div-duc configuration despite the wall shape in its divergent part. With a duc-div configuration, the diffuser presents a dip in the Cp_m curve around L/D=1 for all wall shapes. This dip was also observed by [7] at the inlet of this type of geometry configuration.

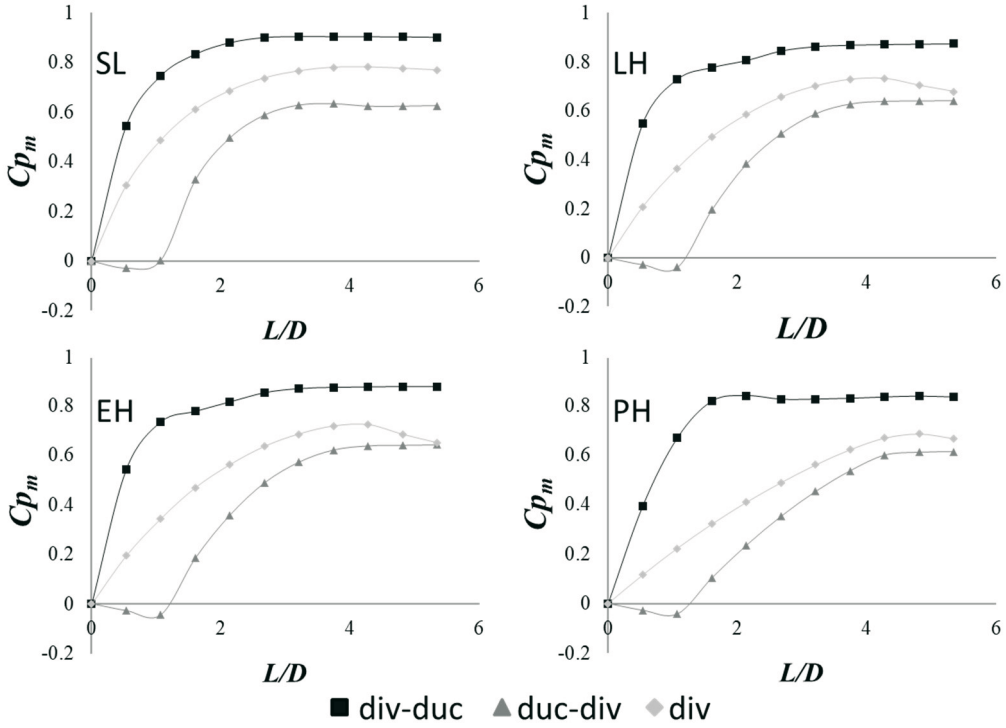

Fig. 7 Mean recovery pressure due to the wall shape using div-duc, duc-div and div configurations

Table 2 presents the Cp_m comparisons obtained by authors applying different optimisation processes and numerical algorithms to find the best diffuser geometry. The value reached in this study by the div-duc configuration with a straight wall is identical to that obtained by [24] when optimising the AR and LR, also using the same design.

Table 2 Comparison of the mean pressure recovery factor obtained by different authors

Author	[18]	[20]	[17]	[22]	[8]	[23]	[15]	[24]	This study
Cp_m	0.718	0.810	0.717	0.817	0.82	0.81	0.714	0.90	0.90

Thus, these results demonstrate that despite the optimisation processes or geometries used by other authors, the diffuser configuration should be the critical factor in obtaining the highest efficiency.

5.2.3 Axial kinetic energy flux

Fig. 8 presents the axial velocity uniformity along the diffuser in response to its configuration and wall shape. Physically, at a given cross section, α represents the ratio of the actual kinetic energy flux to that of the inlet, and it is provided by Eq. 7. A value higher than unity means a non-uniformity of the velocity profile.

This non-uniformity is increased by the divergence at the inlet of the diffuser, regardless of the wall shape used. However, the correct duct length helps to reduce it, reaching almost unity at the exit. This uniformity of the velocity profile drew the highest diffusion values, as

displayed in Fig. 5. Fig. 8 shows that the duct in a diffuser controls the flow non-uniformity; instead, the divergent part increases the flow non-uniformity despite the wall shape used.

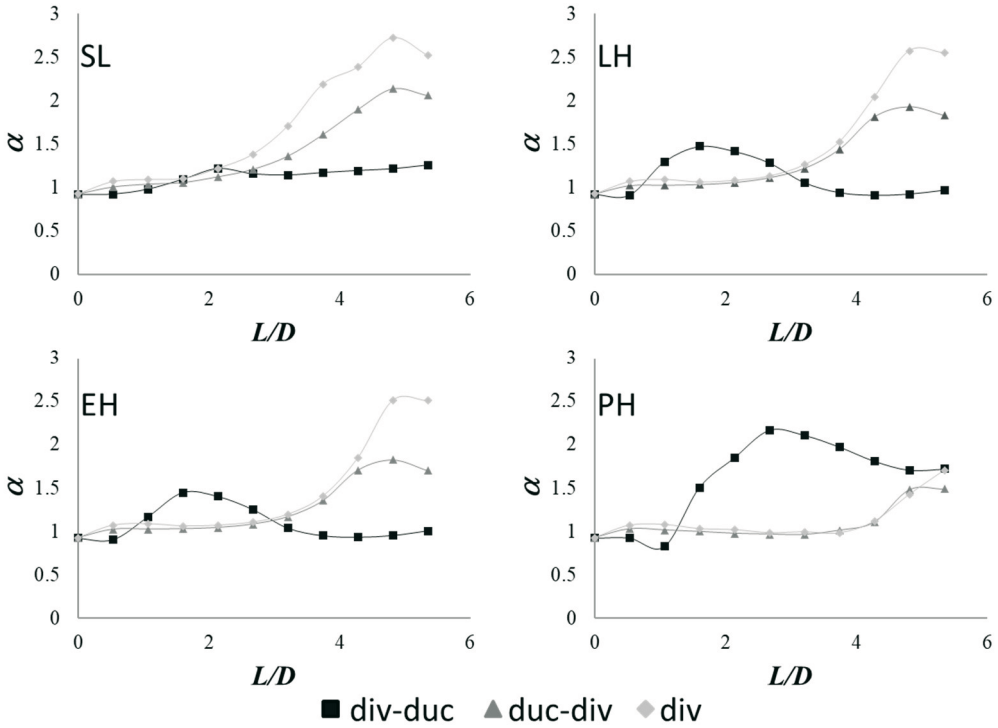

Fig. 8 Axial kinetic energy flux along the diffuser

5.2.4 Swirl intensity

The inlet swirl has a significant impact on diffusers because the flow is directed toward the wall, preventing flow separation. However, excessive swirl reduces the axial velocity near the centre line of the diffuser, inducing a reversed flow region. The swirling number, *S,* defined by Eq. 10, was applied to predict the penetration of the swirl intensity in the downstream cross sections of different geometry configurations.

$$S = \frac{\int_0^R (\rho v_a)(r v_t) r \mathrm{d}r}{R \int_0^R (\rho v_a)(\rho v_a) \mathrm{d}r} \tag{10}$$

Fig. 9 illustrates that the div-duc configuration using a PH wall shape is the only device that can maintain this parameter and increase its value downstream. Conversely, the SL wall shape suffers a slight reduction at the end of the diffuser. The LH and EH wall shapes triggered a wavy behaviour of this quantity, slumping at the end of the device.

When the diffuser begins with a duct, the swirl number decreases, indicating that the divergent part cannot maintain this flow sufficiently energized. Thus, the results show that a more prolonged divergence causes swirl intensity at the inlet of the diffuser but cannot maintain it towards the end of the diffuser.

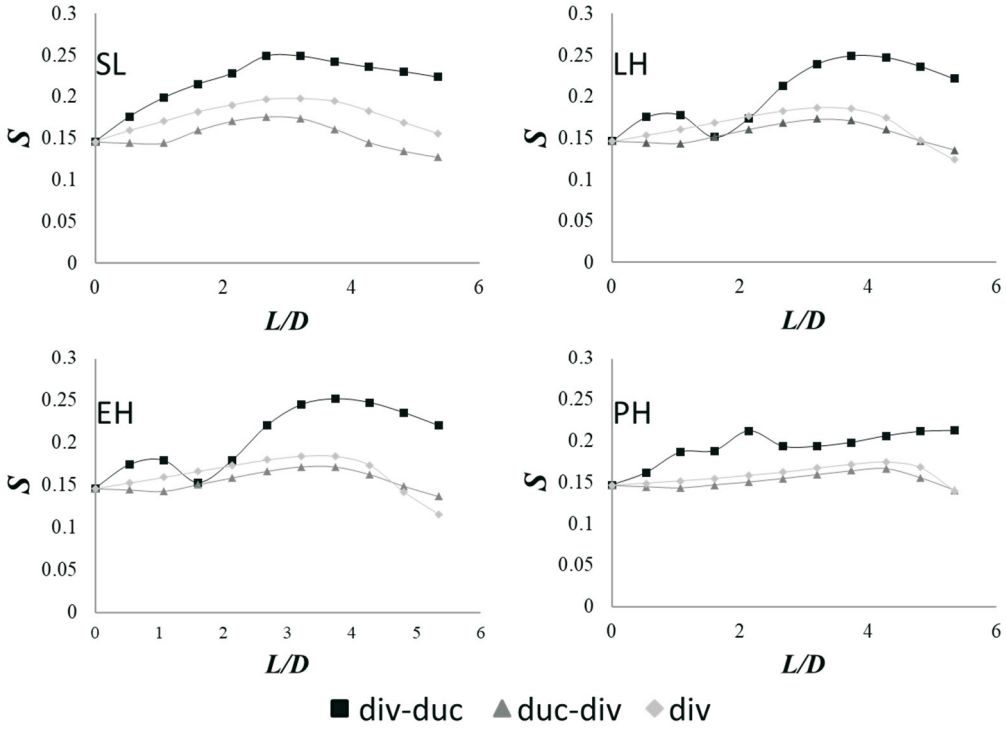

Fig. 9 Behaviour of the swirl intensity of the flow along the diffuser

5.2.5 Tangential shear stress

The variation of the swirl intensity, presented in the previous section, suggests the formation of tangential wall stresses. This non-dimensional parameter, given by Eq. 11, illustrates that the variation of the angular momentum of the fluid flow on a cross section equals the momentum exerted on the fluid flow by the tangential wall shear stress.

$$\tau_w^* = \frac{\mu_t \frac{\mathrm{d}v_t}{\mathrm{d}r}}{\frac{1}{2}\rho\left(\frac{Q}{A_{in}}\right)^2} \tag{11}$$

where $\mu_t = \rho\, C_\mu\, \kappa^2/\varepsilon$.

In Fig. 10, the critical role that the tangential wall shear stress plays on the internal flow field of the diffuser can be observed. The div-duc configuration with any wall shape shows a rapid decline in this value from the inlet of the diffuser to the end of its divergent part. This behaviour is related to the swirl intensity shown in Fig. 9, where the divergence significantly increases these factors. This comparison shows that this diffuser configuration increases the penetration of the inlet swirl intensity that reaches the parallel pipe.

On the other hand, the slope of the shear stresses changes at the inlet of the duc-div configuration, and these stresses are similar despite the wall shape. This same constant decline in the tangential shear stress is reported by [40] where different swirl intensity numbers were used but in a straight pipe.

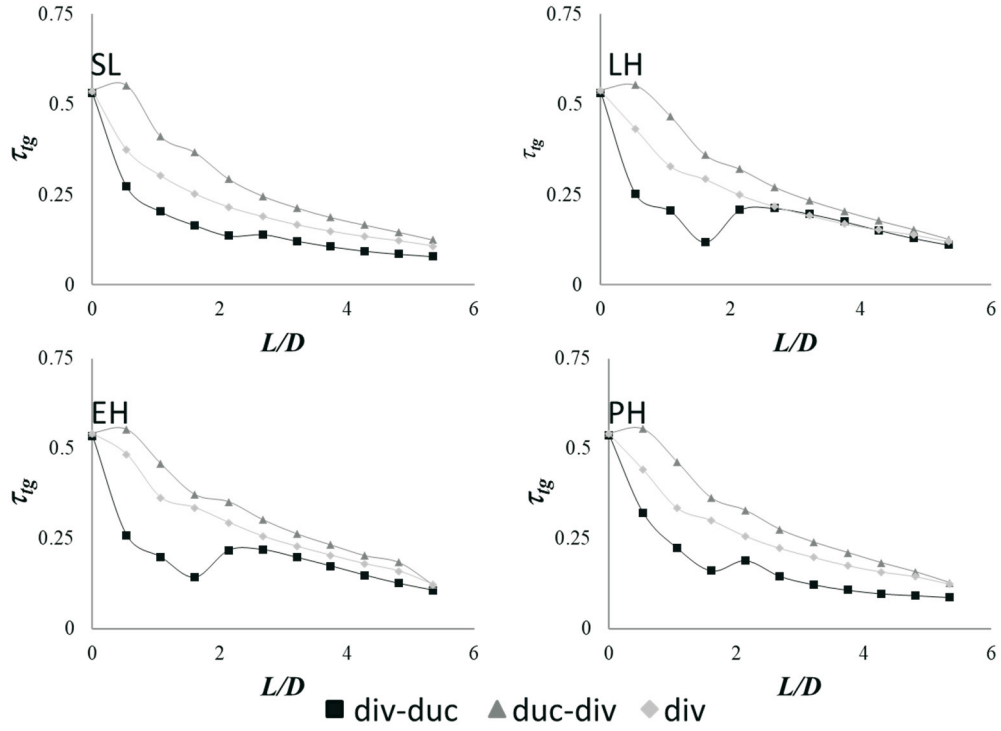

Fig. 10 Tangential wall shear along the diffuser due to the wall shape using div-duc, duc-div and div configurations

5.2.6 Total pressure distribution

Fig. 11 shows the distribution of the total pressure obtained in the meridional plane of each optimal diffuser, estimated as the sum of the static and the dynamic pressure.

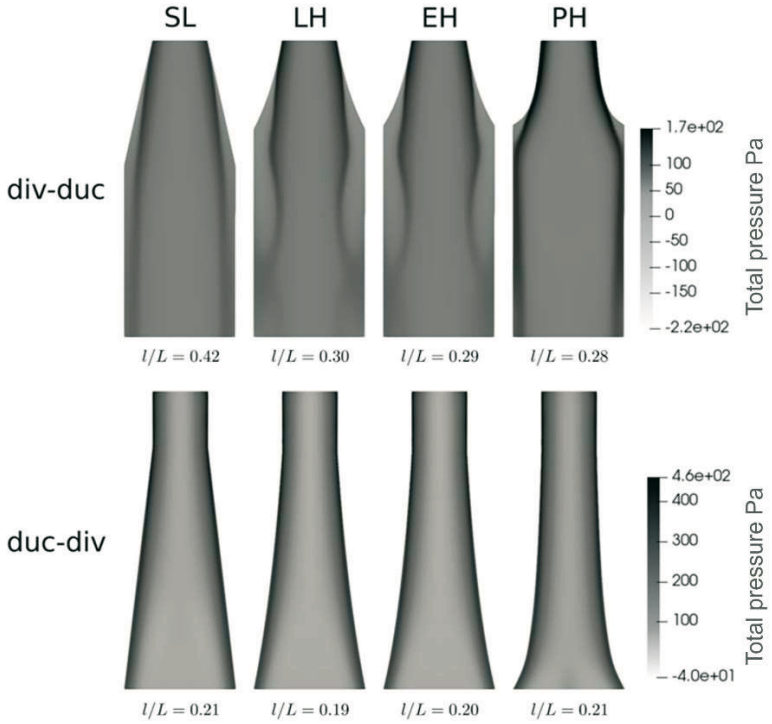

Fig. 11 Pressure contours of the optimised geometries in relation to Fig. 4

In the div-duc configuration (top), the SL wall maintains a uniform pressure field lengthwise due to the homogeneous velocity profile, which stimulates diffusion and reduces

dissipation. For the same configuration, the curved walls (LH, EH) cause fluctuations in the pressure field, increasing dissipation primarily due to the dynamic component. Prasil's hyperbola (PH) wall maintains a smooth pressure contour, but this shape lacks diffusion capacity due to the non-uniform increasing rate of the cross-sectional area. Meanwhile, in the duc-div configurations (bottom), the visualisations do not show irregularities in the pressure field due to the low capacity for diffusion of this diffuser configuration.

Consequently, when geometrical restrictions of the diffuser exist, such as a limited length and area ratio, the performance of the diffuser can be improved using a duct after the divergence to control the non-uniformity of the flow. This exact divergence-duct relation configuration stimulates an efficient diffusion, which will avoid a substantial distortion of the inlet velocity profile, thus resulting in a better performance.

6. Conclusions

This study demonstrated that the divergence placed at the inlet of a diffuser with straight walls and followed by a duct was the geometry that mainly increased the diffusion proportion and minimised the dissipation. Also, with a duct at the diffuser inlet, the wall shapes of the divergent part will have little influence on the reduction of energy losses. Besides, the flow analysis of the best geometries affirmed that the exact length of the divergent part at the inlet of the diffuser not only energized the swirl intensity of the flow, maintaining it in the parallel pipe, but also reduced the tangential wall shear stresses as the flow evolved through the diffuser.

Although the numerical results demonstrate that the re-design of a diffuser improves its efficiency, we should mention some considerations. Firstly, the inlet velocity profiles provided by a runner blade could be very different from those used in this study so that they would restrict the inlet flow to specific characteristics. Secondly, during an optimisation process, where fine details of the flow characteristics were not required, the standard κ-ε turbulence gave reliable results. However, to capture the main features of the flow along the diffuser, the best geometries should be studied using a high-level turbulence model, which will require high-performance computing. And thirdly, the advanced tuning parameters of the MIGA, such as migration or elitism, might diversify the diffuser designs, which will imply reducing the number of islands and generations to minimise the number of CFD evaluations during the optimisation process.

The next step of this methodology should integrate the other two fixed draft tube components into the shape optimisation process and test its efficiency as part of the whole turbine.

Thus, a correct redesign of the diffuser in an already installed plant with cavitation problems could avoid the implementation of guide vanes or air injection at the runner outlet. Also, it could correct the evolution of the mild and high swirling flow created by the newly designed runner when refurbishing a power plant, mainly horizontal (axial) turbines with low head, where the greatest pressure recovery is in the draft tube, avoiding a sudden and unexpected drop in discharge efficiency.

Acknowledgements

The authors gratefully acknowledge the CONAHCYT for the scholarship support to the main author and the *Coordinación de la Investigación Científica* of the *Universidad Michoacana de San Nicolás de Hidalgo* for the financial support to build the computational cluster.

REFERENCES

[1] Susan-Resiga, R.; Muntean, S.; Hasmatuchi, V.; Anton, I.; Avellan, F. Analysis and prevention of vortex breakdown in the simplified discharge cone of a francis turbine, *Journal of Fluids Engineering* **2010**, 132 (5). https://doi.org/10.1115/1.4001486

[2] Ciocan, G.D.; Avellan, F.; Berca, E.L. Wall friction measurements: application in a francis turbine cone, in*: Fluids Engineering Division Summer Meeting* **2002**, pp. 317–322. https://doi.org/10.1115/FEDSM2002-31333

[3] Susan-Resiga, R.; Avellan, F.; Ciocan, G.D.; Muntean, S.; Anton, I. Mathematical and numerical modeling of swirling flow in francis turbine draft tube cone, *Transactions on Mechanics, Scientific Bulletin of the "Politehnica" University of Timisoara* **2005**, *50*, 64, 10–11

[4] McDonald, A.; Fox, R.; Van Dewoestine, R. Effects of swirling inlet flow on pressure recovery in conical diffusers, *AIAA Journal* **1971**, 9 (10), 2014–2018. https://doi.org/10.2514/3.6456

[5] Klein, A. Review: Effects of Inlet Conditions on Conical-Diffuser Performance, *Journal of Fluids Engineering* **1981**, 103 (2), 250–257. https://doi.org/10.1115/1.3241727

[6] Senoo, Y.; Kawaguchi, N.; Nagata, T. Swirl flow in conical diffusers, *Bulletin of JSME* **1978**, 21, 151, 112–119. https://doi.org/10.1299/jsme1958.21.112

[7] Sharan, V.K. An exponential investigation of the behavior of conical diffusers in turbulent flow, *Journal of Applied Mathematics and Physics (ZAMP)* **1976**, 27, 447–462. https://doi.org/10.1007/BF01594901

[8] Khare, R.; Prasad, V.; Verma, M. Design optimisation of conical draft tube of hydraulic turbine, *IJAEST International Journal of Advances in Engineering, Science and Technology* **2012**, 2(1), 22-26

[9] Karki, B.; Ghimire, S. K.; Dura, H. B. Design & Study of Conical Draft Tube For Francis Turbine For Steady Flow. *Proceedings of 8th IOE Graduate Conference* **2020**, Volume: 8

[10] Jha A.; Muchrika A. Geometrical optimization of diffuser under swirl flow inlet condition using CFD analysis, *International Journal of Engineering Development and Research* **2020**, Volume8, Issue3

[11] Agarwal, A.; Mthembu, L. CFD analysis of conical diffuser under swirl flow inlet conditions using turbulence models, *Materials Today: Proceedings* **2020**, vol. 27, p. 1350-1355. https://doi.org/10.1016/j.matpr.2020.02.621

[12] JIAO, Weixuan, et al. Investigation of Key Parameters for Hydraulic Optimization of an Inlet Duct Based on a Whole Waterjet Propulsion Pump System. Transactions of FAMENA, 2021, vol. 45, no 1, p. 145-162. https://doi.org/10.21278/TOF.451004819

[13] Daniels, S. J., et al. Application of multi-objective Bayesian shape optimisation to a sharp-heeled Kaplan draft tube, *Optimization and Engineering* 2021, p. 1-28. https://doi.org/10.1007/s11081-021-09602-6

[14] Perišić, Stipe, et al. A Bayesian Conjugate Model for the Estimation of Friction Intensity. *Transactions of FAMENA* **2021**, vol. 45, no 1, p. 63-77. https://doi.org/10.21278/TOF.451026321

[15] Thévenin, D.; Janiga, G. Optimization and computational fluid dynamics. *Springer Science & Business Media* **2008**. https://doi.org/10.1007/978-3-540-72153-6

[16] Fares, R.; Chen, X.; Agarwal, R. Shape optimization of an axisymmetric diffuser and a 3D hydro-turbine draft tube using a genetic algorithm. In 49th AIAA Aerospace Sciences Meeting including the New Horizons Forum and Aerospace Exposition 2011, (p. 1243). https://doi.org/10.2514/6.2011-1243

[17] Djebedjian, B. O. Diffuser Optimization Using Computational Fluid Dynamics and Micro-Genetic Algorithms, MEJ Mansoura Engineering Journal 2021, 28(4), 15-34. https://doi.org/10.21608/bfemu.2021.142398

[18] Ghosh, S.; Pratihar, D.; Maiti, B.; Das, P. An evolutionary optimization of diffuser shapes based on CFD simulations. International journal for numerical methods in fluids 2010, 63 (10), 1147–1166. https://doi.org/10.1002/fld.2124

[19] Madsen, J.I.; Shyy, W.; Haftka, R.T. Response surface techniques for diffuser shape optimization. AIAA journal 2000, 38 (9), 1512–1518. https://doi.org/10.2514/2.1160

[20] Shojaeefard, M.H.; Mirzaei, A.; Babaei, A. Shape optimization of draft tubes for Agnew microhydro turbines. *Energy Conversion and Management* **2014**, 79, 681–689. https://doi.org/10.1016/j.enconman.2013.12.025

[21] Marjavaara, B.D.; Lundström, T.S.; Goel, T.; Mack, Y.; Shyy, W. Hydraulic turbine diffuser shape optimization by multiple surrogate model approximations of pareto fronts, *Journal of Fluids Engineering* **2007**, 129 (9), 1228–1240. https://doi.org/10.1115/1.2754324

[22] Rudolf, P. Optimization methods for hydraulic machines design-shape optimization of swirl turbine draft tube, In *Conference paper–Hydroturbo* **2006**

[23] Rudolf, P.; Nemec, T.; Performance improvement of a short draft tube, in: *Proceeedings of the conference Power System Engineering, Pilsen* **2008**

[24] Moravec, P., Hliník, J., & Rudolf, P. Optimization of hydraulic turbine diffuser. In *EPJ web of conferences* **2016**, (Vol. 114, p. 02079). EDP Sciences. https://doi.org/10.1051/epjconf/201611402079

[25] Herrera, N.; Galván, S.; Camacho, J.; Solorio, G.; Aguilar, A. Automatic shape optimization of a conical-duct diffuser using a distributed computing algorithm. *Journal of the Brazilian Society of Mechanical Sciences and Engineering* **2017**, 39, 4367–4378. https://doi.org/10.1007/s40430-017-0753-5

[26] Engineous Software Inc. Products **1994**, Isight

[27] The Math Works, Inc. **2005**, Matlab

[28] Fluent Inc. **2007**, Gambit

[29] Fluent Inc. **2016**, Fluent

[30] Gubin, M.F. Draft tubes of hydro-electric stations, *Amerind Publishing Company for the US Bureau of Reclamation* **1973**

[31] Galván, S., Rubio, C., Pacheco, J., Gildardo, S., & Carbajal G. Optimization methodology assessment for the inlet velocity profile of a hydraulic turbine draft tube: part II—performance evaluation of draft tube model. Journal of Global Optimization, **2013**, 55, 729-749. https://doi.org/10.1007/s10898-012-0011-4

[32] Zhang, X., Gan, H., Xue, H. & Jiang, Q. Numerical Simulation of an Experimental Study on Structure Optimization for Compartment Dryers. *Transactions of FAMENA* **2024**, Vol 48, no 3, p. 95-110. https://doi.org/10.21278/TOF.483057623

[33] Galván, S.; Reggio, M.; Guibault, F. Optimization of the inlet velocity profile in a conical diffuser. En *Fluids Engineering Division Summer Meeting. American Society of Mechanical Engineers* **2012**. p. 125-134. https://doi.org/10.1115/FEDSM2012-72103

[34] Galván, S.; Rubio, C.; Pacheco, J.; Mendoza, C.; Toledo, M. Optimization methodology assessment for the inlet velocity profile of a hydraulic turbine draft tube: part I - computer optimization techniques, *Journal of Global Optimization* **2013**, 55, 53–72. https://doi.org/10.1007/s10898-012-9946-8

[35] Tanriver, K. & Ay, M. Efficient Path Planning for Drilling Processes: The Hybrid Approach of a Genetic Algorithm and Ant Colony Optimisation. *Transactions of FAMENA* **2024**, vol. 48, no 3, p. 125-140. https://doi.org/10.21278/TOF.483062023

[36] Harikrishnan, V.K., Annamalai, S., Sampath, S. & Paramasivam, S. A Time-Performance Improvement Model with Optimal Ergonomic Risk Level Using Genetic Algorithm. *Transactions of FAMENA* **2023**, vol. 47, no 4, p. 109-128. https://doi.org/10.21278/TOF.474049022

[37] Moses, H.L. Diffuser performance for draft tube applications, in: *Waterpower'85, ASCE* **1986**, pp. 1218–1227

[38] Molinero, D.; Galván, S.; Pacheco, J.; Herrera, N. Multi gpu implementation to accelerate the cfd simulation of a 3d turbo-machinery benchmark using the rapidcfd library, in: *International Conference on Supercomputing in Mexico, Springer* **2019**, pp. 173–187. https://doi.org/10.1007/978-3-030-38043-4_15

[39] Tuković, Ž.; Karač, A.; Cardiff, P.; Jasak, H.; Ivanković, A. OpenFOAM finite volume solver for fluid-solid interaction. *Transactions of FAMENA* **2018**, vol. 42, no 3, p. 1-31. https://doi.org/10.21278/TOF.42301

[40] Najafi, A., Mousavian, S., Amini, K. Numerical investigations on swirl intensity decay rate for turbulent swirling flow in a fixed pipe. *International Journal of Mechanical Sciences* **2011**, 53, 801–811. https://doi.org/10.1016/j.ijmecsci.2011.06.011

Submitted: 29.4.2023

Accepted: 17.02.2025

Nicolás Herrera-Sandoval
Cristóbal Camacho-Arriaga
Tecnológico Nacional de México, campus Morelia, Morelia, Michoacán, Mexico
Daniel Molinero
Sergio Galván-González*
Carlos Rubio-Maya
Jesús Pacheco-Ibarra
Universidad Michoacana de Sán Nicolás de Hidalgo, Mechanical Engineering Faculty, Morelia, Michoacán, Mexico
*Corresponding author:
sergio.galvan@umich.mx